



Royal Netherlands
Meteorological Institute
*Ministry of Infrastructure
and Water Management*

Winschoten events, 19-11-2017

E. Ruigrok, J. Spetzler, B. Dost and L. Evers

De Bilt, 2018 | Technical report; TR-368

Winschoten events, 19-11-2017

KNMI, Dept. R&D Seismology and Acoustics

Elmer Ruigrok, Jesper Spetzler, Bernard Dost and Láslo Evers

August 28, 2018

Summary

A succession of at least 4 events was measured on November 19, 2017, close to the city of Winschoten, at the south-eastern edge of the Groningen gas field. The largest amplitude recorded was at sensor G570: a peak particle acceleration of 2.45 mm/s. The waveforms had a signature different from the events initiated in the vicinity of the gas reservoir. Moreover, the Groningen gas field had not been seismically active at the south-eastern edge of the field. An alternative seismic source would be deformation in a salt cavern. The preliminary epicentre of the main event was situated on top of the Heiligerlee salt dome, in which 12 salt caverns have been mined. With a better constrained location and a spectral analysis, we assess whether the salt-cavern hypothesis is likely.

Using 5 improved P-wave picks and a detailed 3D velocity model for the area, the main event was mapped to a source location in the (lower) North Sea Group or upper Chalk Group, above the western flank of the Heiligerlee salt dome. At this location, brittle rock overlying the salt dome could have moved due to salt creep. The uncertainty ellipse includes the part of the salt dome where the caverns are present. However, a hypocentre at the depth range of the caverns is unlikely. With the assumption that the source is just within the Chalk Group, a moment magnitude of 1.28 ± 0.08 is found.

All nearby KNMI seismic stations recorded a strong 3.4 Hz resonance for the event. Due to large differences in receiver-side structure, the 3.4 Hz resonance likely originated from the source area. The assumption was tested whether one of the salt caverns would act as a resonating closed pipe. From the 12 caverns, 2 can possibly generate the recorded resonance: brine filled cavern HL-M over its height and nitrogen-filled cavern HL-K over its width. Another possible resonator, which is more in-line with the updated source location, would be the lower North Sea Group in the source area.

Waveforms two weeks prior to two weeks after November 19 were scanned to find possible similar, but smaller, events. The two largest subevents (W2 and W3) were used as a template. The scanning resulted in a few records with similarities just above the threshold of a 0.5 correlation coefficient. Subevent W4 turned out to be a close match to W3, with a correlation coefficient of 0.65.

The implemented scanning approach is not sufficient as a monitoring tool. Events are likely to occur for which a template does not yet exist. For detailed seismic monitoring of the Heiligerlee salt dome, currently there is no dedicated network, to allow both detection and location of very small seismic events. As a (temporary) alternative, we would suggest a monitoring tool solely based on sliding windows of root-mean-square amplitudes.

1 Introduction

On November 19, 2017 an event was recorded at seismic stations near Winschoten, at the south-eastern edge of the Groningen gas field. For locating the event, initially the operational procedure was followed, assuming an earthquake near reservoir level. This resulted in a large misfit. Also the signature of the event did not match with known events at reservoir level: the Winschoten event had a less balanced frequency spectrum and a smaller time difference between the first P- and S-wave arrivals than observed for events around 3 km depth, i.e., at reservoir level. Moreover, the gas field had not been seismically active near Winschoten. Changing the assumption from a reservoir source to a source near the Earth's surface, a much better location was obtained. The nature of this source, however, remained unknown.

In this report we implement a dedicated processing to find a better constrained location and characteristics of the event. A hypothesis would be that the seismic source is related to salt caverns which have been mined at the north-eastern edge of Winschoten, in the Heiligerlee salt dome. With a better constrained location and a spectral analysis, we assess whether such hypothesis is likely.

A controlled (*Kinscher et al.*, 2014) and uncontrolled (*Shemeta et al.*, 2013) collapse of a salt cavern were seismically monitored. In both cases a large amount of seismicity was observed prior to the actual collapse. If the event detected near Winschoten is related to a salt cavern, monitoring a possible build-up of seismicity would allow to warn for possible hazardous situations. We use the recorded events as templates and scan through the continuous data prior and after the main event to find possibly previously undetected small-sized events from a similar source region. To detect also the build-up of events for which there are no templates, we test the use of a root-mean-square amplitude tracker.

2 Observations

The Winschoten event resulted in the largest recorded ground shaking at surface sensor G570, which is part of the KNMI seismic network (*Dost et al.*, 2017). Fig. 1 shows the recording at this accelerometer, expressed in particle velocity and particle acceleration. Fig. 2 shows the location of station G57, consisting of a sensor at the Earth's surface: G570, and 4 at depth: G571-G574, ranging from 50 to 200 m. The largest amplitude was recorded on the north-component of G570, a peak particle velocity of 48.7 m/s and a peak particle acceleration of 2.45 mm/s. The latter corresponds to 0.0245% of g (gravitational acceleration near the Earth's surface).

P-waves were picked and the event was located using the operational system at KNMI: SeisComp3 (www.seiscomp3.org). For the location, an implementation of the hypocentre method as described by *Lienert et al.* (1986), was used. The best location was obtained by assuming it to be a source near the Earth's surface, instead of near the gas reservoir. Fig. 2 shows this location as obtained with Hypocentre. Although the event is located within the gas-water polygon of the Groningen gas field, it is within an area that has not been seismically active before (Fig. 2a). However, it is close to the apex of the Heiligerlee salt dome (Fig. 2b).

Fig. 3 shows the source gather for the Winschoten event. The strongest package of waves can still be seen beyond 14 km distance. Only the onsets of these strongest arrivals were picked. The resulting earthquake origin time (EOT), is the zero time on this graph. It can be seen that there are coherent arrivals before this EOT.

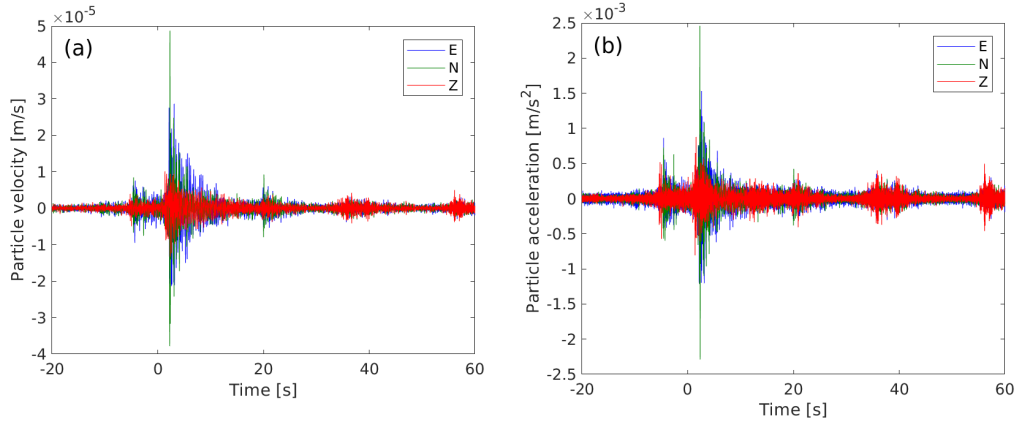


Figure 1: 3-component recordings at sensor G570, expressed in (a) particle velocity and (b) particle acceleration. E, N and Z denote east, north and vertical movements, respectively. The zero time corresponds to the Hypocentre earthquake origin time of the main event: 19-11-2017 14:00:48 UTC (15:00:48 local time).

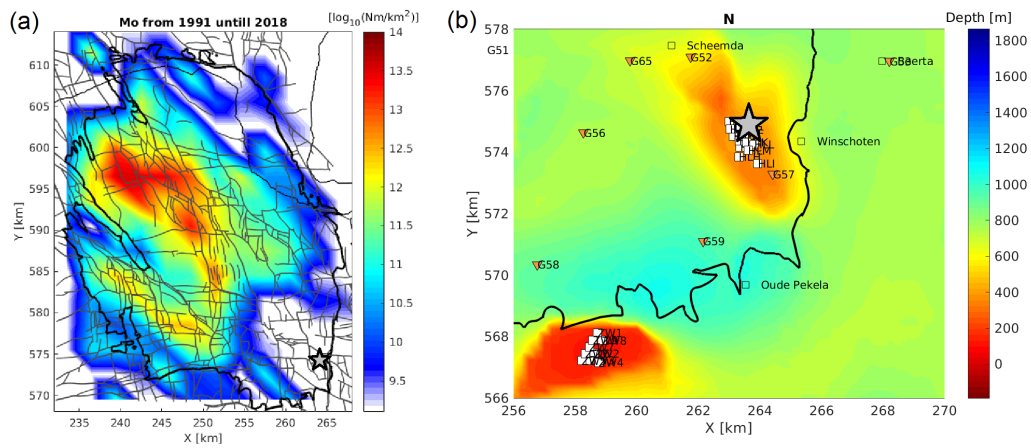


Figure 2: (a) Distribution of the total seismic moment release (colour map) over the Groningen gas field (black solid line) between 1991 and January 2018, and the Hypocentre source location (grey star) for the 19-11-2017 event. Faults at reservoir level are denoted by grey lines. (b) Area of interest around Winschoten, with the source location (grey star) and KNMI seismic stations (orange triangles) indicated. The colour map shows the depth of the North Sea Group, with two highs (red) where salt domes exist. White squares denote salt caverns (Appendix A) and the black solid line shows the south-eastern edge of the Groningen gas field.

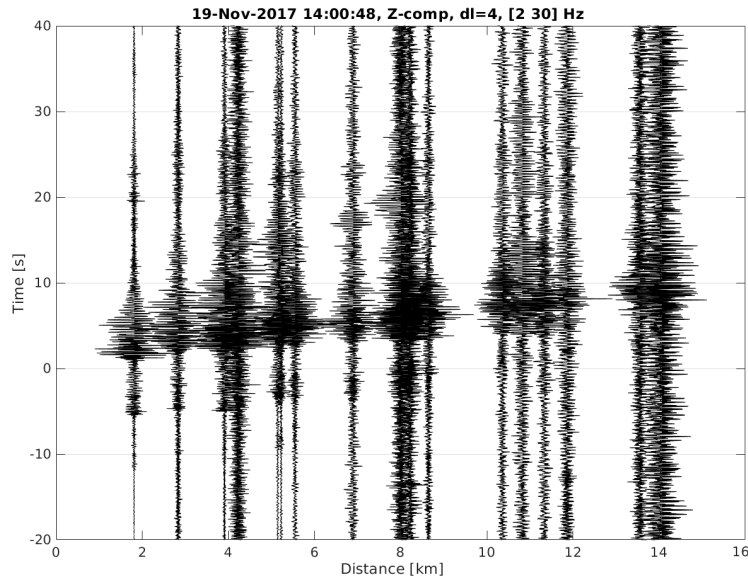


Figure 3: Event gather of vertical-component particle velocity recordings at 200 m depth, frequency band-pass filtered between 2 and 30 Hz.

Fig. 4 shows the seismograms at two most nearby stations, at the 200 m depth level, both in the time and the frequency-time domain. After closer inspection at least 4 (sub)events can be distinguished, two before the main (and located) event and one after.

The initial picks were made with SeisComp3 using only the sensor at 200 m depth. Picking of the P-wave onset of the main event is difficult, because coda from the previous event is still concurrently being recorded. The picking is improved by analysing the data in different frequency bands. Only the onset of P-wave from the most recent event is still enriched in higher frequencies, while for the coda of the older events the high frequency part of the waves has already been attenuated. Moreover, the picking is made easier by selecting consistent onsets over all the depth levels of one station. This depth-consistent picking can be done by knowing the interval velocities along the borehole (*Hofman et al., 2017*) and by taking advantage of the near-vertical incidence of the first P- and S-wave. At close range (stations G52 and G57), deviation from near-vertical propagation may be expected, but also here the first P- and S-wave onsets follow the move-outs for vertically travelling upgoing waves.

Figs. 5–7 show 3-component recordings of the main event (the most energetic) at all nearby stations at which the P-wave onset could be identified. Only at the two most nearby stations, G57 and G52 (Fig. 2b) also the S-wave onset could be picked with confidence. The timing of the picks (at the 200 m depth level) are indicated in the figures. These timings are used in the next section to improve the location.

3 Location

In the first stance, we improve the epicentre of the main event, by using the improved P-wave picks (see previous section). Afterwards, we use the time difference between the P- and S-wave onsets at the two nearest stations to make a maximum depth estimate. Our final solution uses 3D raytracing through a recently updated 3D velocity model of the area.

Prior to relocation, a jack-knife procedure is done to find picks that are inconsistent with the

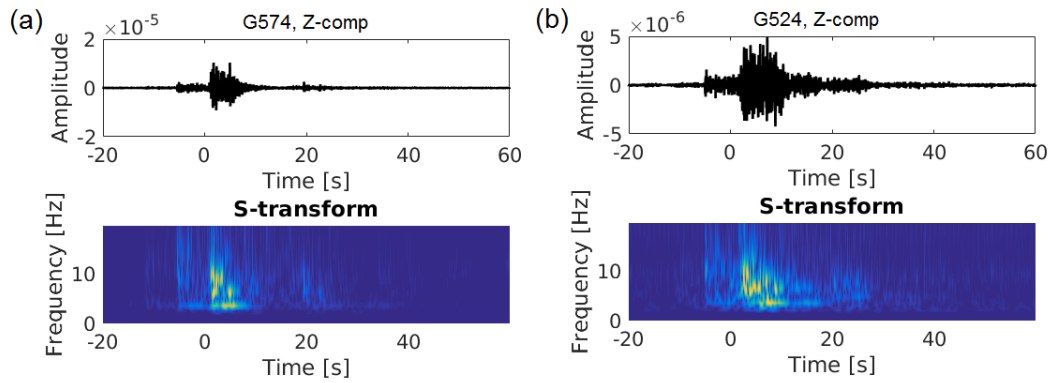


Figure 4: Recording of the Winschoten 19-11-2017 events at the two nearest sensors at 200 m depth: (a) G574 and (b) G524. The upper panels show registrations in the time domain, the lower ones show the recordings mapped to the time-frequency domain using the S-transform (*Stockwell et al., 1996*).

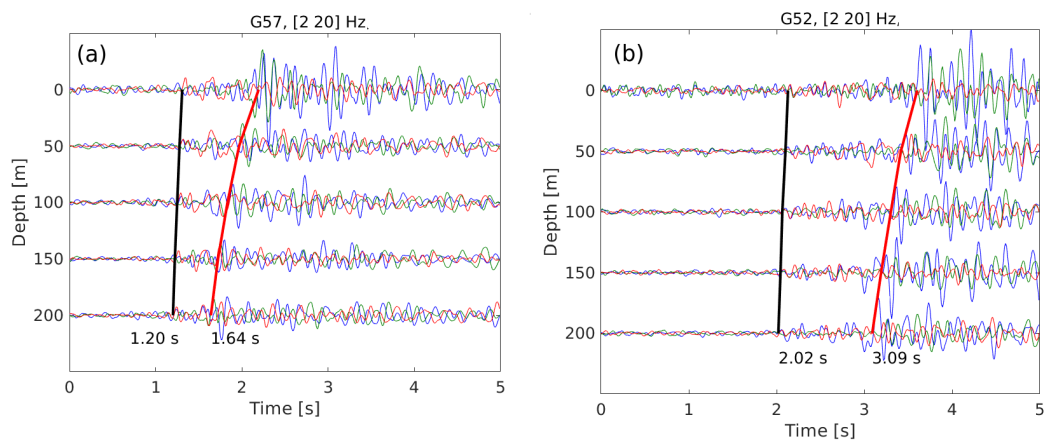


Figure 5: 3-component response at 5 depth levels in boreholes (a) G57 and (b) G52. The red, blue and green seismograms denote the vertical, radial and transverse particle velocity recordings. Thick black and red lines denote depth-consistent picks of the first P- and S-wave onset, respectively.

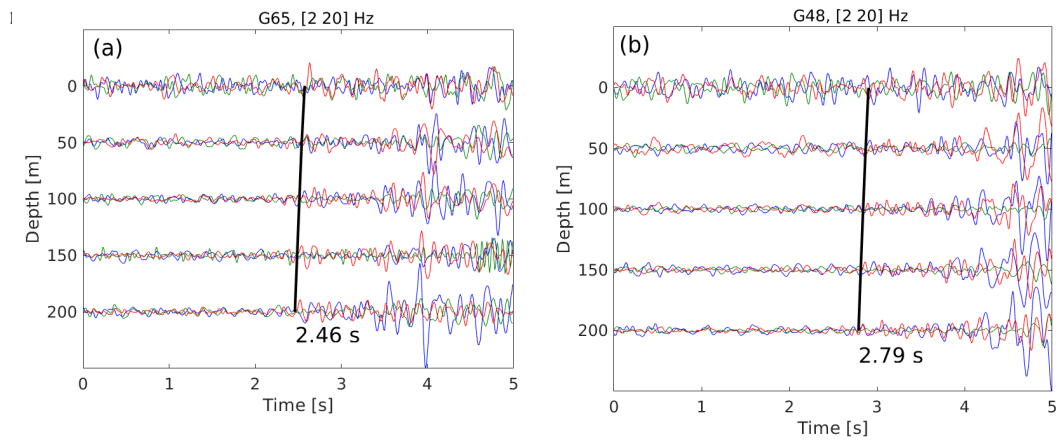


Figure 6: 3-component response at 5 depth levels in boreholes (a) G65 and (b) G48. The red, blue and green seismograms denote the vertical, radial and transverse particle velocity recordings. Thick black lines denote depth-consistent picks of the first P-wave onset. Geophone G653 (depth level 150 m) has malfunctioning horizontal components.

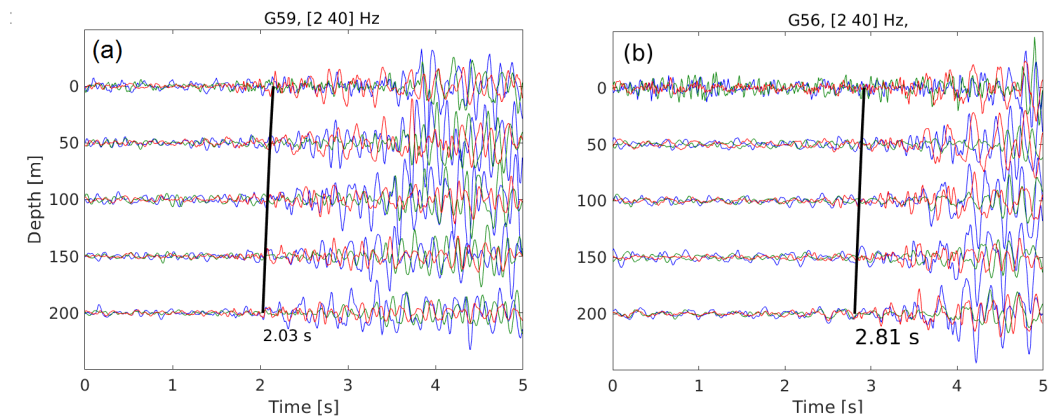


Figure 7: 3-component response at 5 depth levels in boreholes (a) G59 and (b) G56. The red, blue and green seismograms denote the vertical, radial and transverse particle velocity recordings. Thick black lines denote depth-consistent picks of the first P-wave onset.

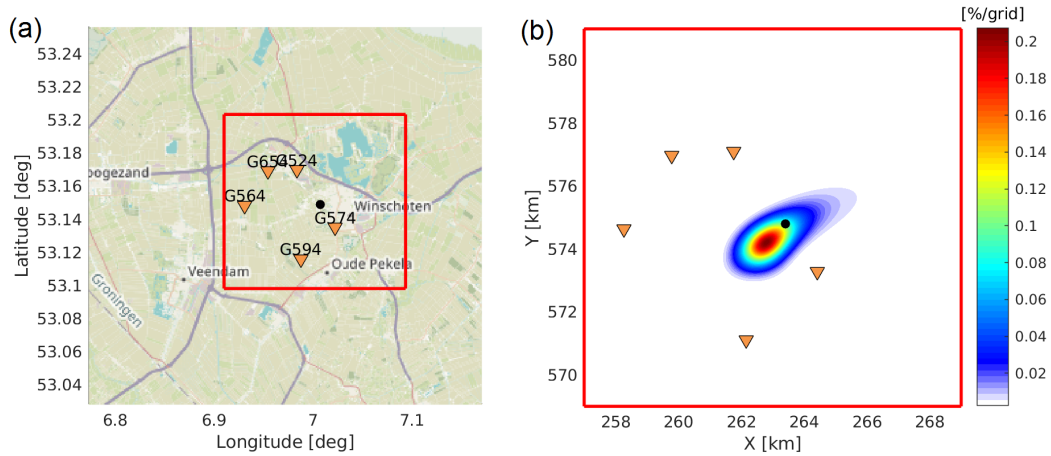


Figure 8: (a) Overview map with locations of stations (yellow triangles) where P-wave onsets were picked, the fast Hypocenter solution (black dot) and the boundary line of the area in which a grid search is done (red box). Background map is from www.openstreetmap.org. (b) probability density function for the epicentre, obtained with the improved picks. The colour bar encompasses the 95% confidence region.

other picks. At larger range both the pick certainty degrades and the used velocity model has a higher chance to accrue errors. It is found that G484 remains to have large residuals at locations where travel times at the other 5 stations are quite well explained.

The epicentre is estimated using a time difference algorithm (*Lomax, 2005*). This approach is abbreviated as equal differential time (EDT). Fig. 8(a) shows the nearby geophones at which a confident P-wave pick could be made (orange triangles) and the initial Hypocentre location (black dot). A grid search is done within the area bounded by the red line. Fig. 8(b) shows the resulting probability density function for the epicentre and the new location, which is the position where the largest probability is reached. This relocation is tabulated in Table 1. For computing the PDF it is assumed that each arrival has a standard deviation σ of 0.4 seconds. This σ both expresses uncertainty in the velocity model and in the picking.

After improving the P-wave picks and implementing the EDT method, the epicentre has moved a few hundred meters to the west. However, the probability density function (PDF) has a high confidence area over most of the minor axis of the salt dome. The location could be further improved if a traveltime table were used that honours the large 3D velocity variations in the subsurface.

Both the Hypocentre and the EDT epicentre are close to a straight line between stations G52 and G57 (Fig. 8b). For these two stations, both the P-wave and S-wave onset could be picked (Fig. 5). In the following we use the differential P-S delay times at these two stations to obtain a maximum depth estimate of the main event.

Fig. 9 shows a section of the Velmod-3 velocity model (*Van Dalfsen et al., 2006*) between stations G52 (upper left corner) and G57 (upper right corner). The assumption is made that the event is located within this section. The P-S delay time for geophone G524 is mapped to an isochron (red line) which shows all positions that would result in the recorded P-S delay time at G524. Similarly, the blue line shows the isochron line for the P-S delay time at G574. The intersection of both isochron lines gives an estimate of the hypocentre. The new location is tabulated in Table 1. The depth estimate of 1.5 km can be seen as a maximum depth. If the source is moved to a position away from the vertical section between stations

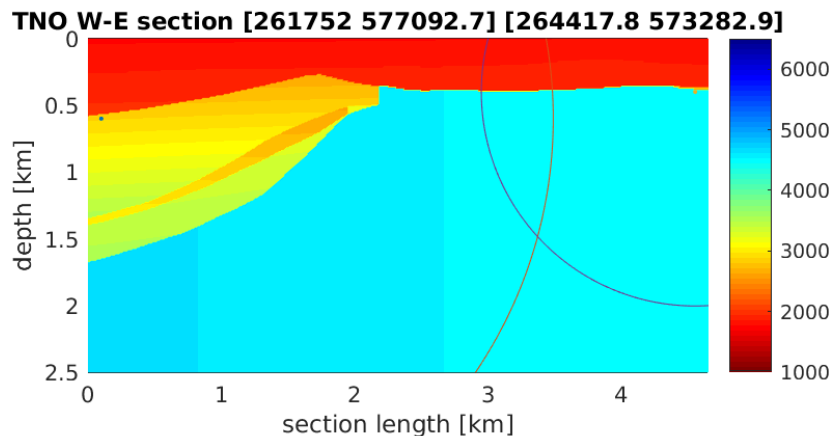


Figure 9: Section through Velmod-3 (*Van Dalfsen et al.*, 2006) between stations G52 and G57 of the KNMI network (*KNMI*, 1993). The colour map shows P-wave velocities in m/s. Blue correspond to mostly halite deposited in the Perm, yellow-to-green corresponds to chalk from the Cretaceous and red corresponds to mostly unconsolidated sediments from the Paleogene and Neogene. The red and blue line show P-S delay isochrones for geophones G524 and G574, respectively. The intersection of the two lines is an estimate of the hypocentre.

G52 and G57, a shallower depth is obtained.

To further improve the location, it is required to honour the complicated 3D velocity model. A detailed P- and S-wave velocity model is available for the Groningen area (*Romijn*, 2017), including the Heiligerlee and Zuidwending salt domes. A 3D ray tracer (*Snieder and Sambridge*, 1992) in combination with a conjugate gradient method has been implemented and is currently in test mode for Groningen seismicity (*Spetzler et al.*, 2018).

The 3D EDT method is implemented for the Winschoten main event, using the P-wave picks in Figs. 5–7. Again, the pick at G484 is omitted as it turned out to be worst-in-class in a jack-knife test. A cube is sampled that covers a wide area around the salt dome; the lateral sampling is 439 m and the vertical sampling is 100 m. For each grid point, the residual is computed (observed traveltimes minus forward modelled traveltimes).

For the remaining 5 stations, the 3D EDT traveltimes residuals are computed for the P-wave picks; for each grid point, and for each station combination, the observed traveltimes differences minus forward modelled traveltimes differences are tabulated. From the 3D EDT residuals, the probability density function (PDF) is derived (*Tarantola*, 2005) using an l_1 norm. Marginal PDFs are shown in Fig. 10.

Fig. 10(a) shows the marginal PDF for the horizontal plane. A minimum in the misfit function leads to a maximum in the PDF. Two maxima are present. The global maximum is located within the polygon formed by the 5 stations with usable picks. The other maximum lies northeast of station G52. To determine the depth of the event, the solution space is sampled for all positions within the station polygon. Fig. 10(b) shows the highest probability reached at each depth. This probability distribution has the largest values for the upper 5 depth intervals (0 to 400 m). The largest probability resides at the free surface, however there is another local maximum at 400 m depth. We select this second maximum since it better fits with our other observations: no surface expressions were reported and the first onsets were upgoing P- and S-waves at all 6 stations (Figs. 5–7).

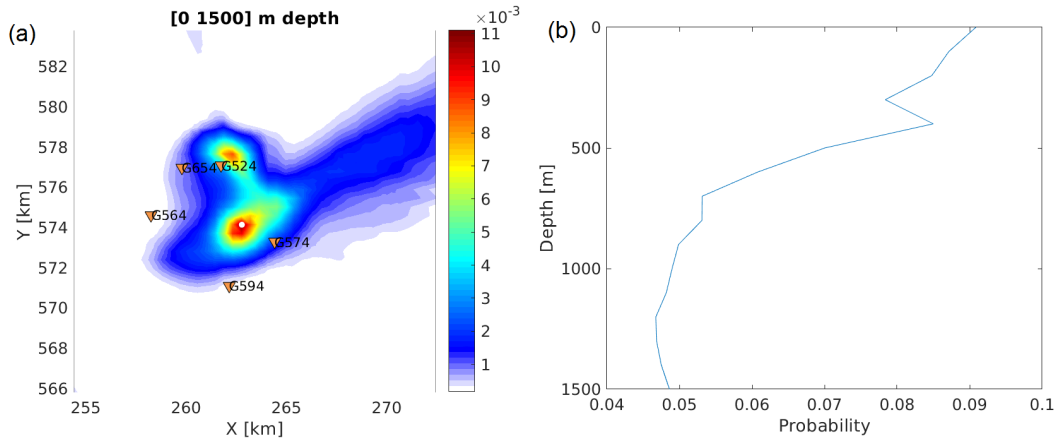


Figure 10: (a) marginal epicentral probability density function. Red denotes high probability. The colour scale covers the 95% confidence area. (b) Event location probability as function of depth

Method	Model	RDx [km]	RDy [km]	Lon [°]	Lat [°]	(max) depth [km]
Hypocenter	1D	263.4	574.8	7.008	53.149	-
EDT	1D	262.8	574.0	6.999	53.144	-
P-S delay	2D	263.6	574.4	7.011	53.145	1.5
3D EDT	3D	262.8	573.7	6.998	53.139	0.4

Table 1: locations obtained for the main event using different data attributes, methods and velocity models.

Fig. 11(a) shows the PDF slice at 400 m depth and the picked event location (white spot). This is the 3D EDT hypocentral solution as tabulated in Table 1. Fig. 11(b)&(c) show the location in their regional context. On Fig. 11(c) it can be seen that the event is situated near the boundary between the North Sea Group (with velocities indicated in red) and the Chalk Group (with a strong velocity gradient indicated with colours ranging from orange to green). The event is located at a position above the western flank of the Heiligerlee salt dome. On Fig. 11(b) it can be seen that the uncertainty ellipse covers all salt caverns in the Heiligerlee dome. A hypocentre within the depth range of the salt caverns is unlikely, however (Fig. 10b and Figs. A.2 & A.3).

It is checked whether the 3D EDT epicentre is consistent with the observed P-wave polarization. Fig. 12 shows the dominant directionality in a window around the P-wave arrival (black arrows) and the radial directionality in case of a 1D velocity structure (green arrows). It can be seen that at the two stations south of the 3D EDT location, there is no good match between the observed and radial polarization. This can be explained by the presence of large 3D variations in the velocity field (salt dome). At most other stations there is a very good match.

The 3D EDT event location is above the steep western flank of the Heiligerlee salt dome (Fig. 11c). At this location, halite is overlain by more brittle rock, which could have slid due to stress build up by salt creep. The North Sea Group contains primarily unconsolidated material. Hence, from a geomechanical perspective, an event location just within the Chalk Group would be more likely than within the North Sea Group.

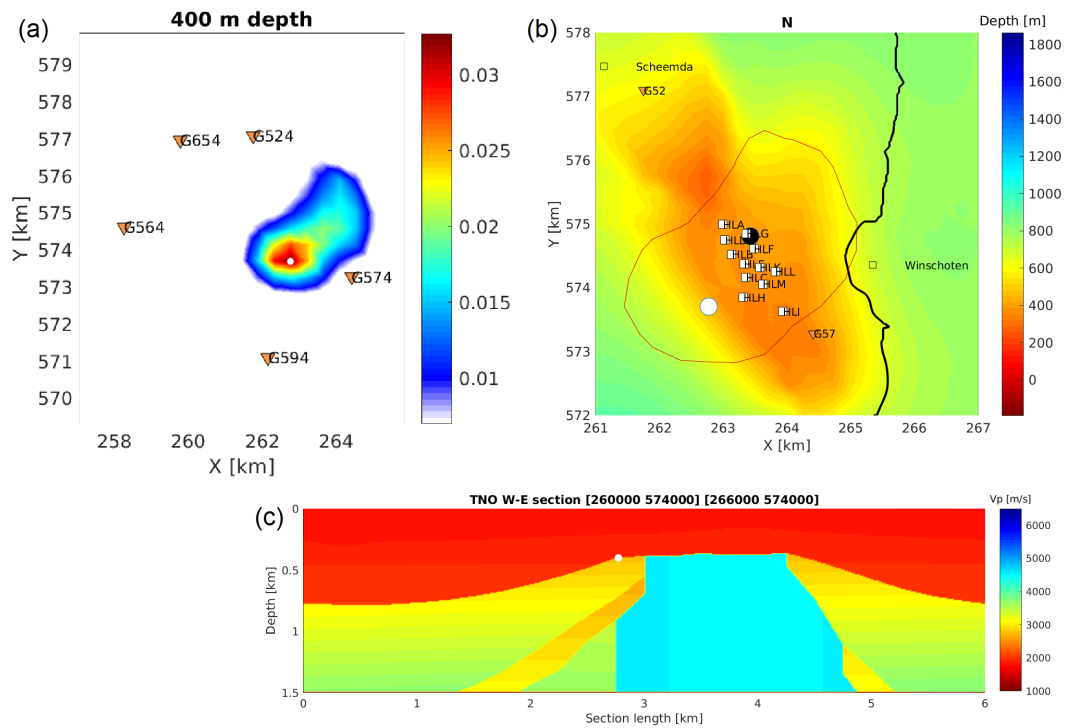


Figure 11: (a) 3D EDT PDF slice near the free surface. The coloured probabilities cover the 95% confidence area. (b) Map view of 3D EDT location (white dot) in context of the Hypocentre location (black dot), the cavern locations (white squares) and a depth map of the North Sea Group (colour map). The outline of the 95% confidence area is plotted with a red line. (c) the 3D EDT location (white dot) on top of a vertical slice through the 3D P-wave velocity model (*Van Dalssen et al., 2006*). The Heiligerlee salt dome corresponds with primarily halite P-wave velocities, which are shown in cyan.

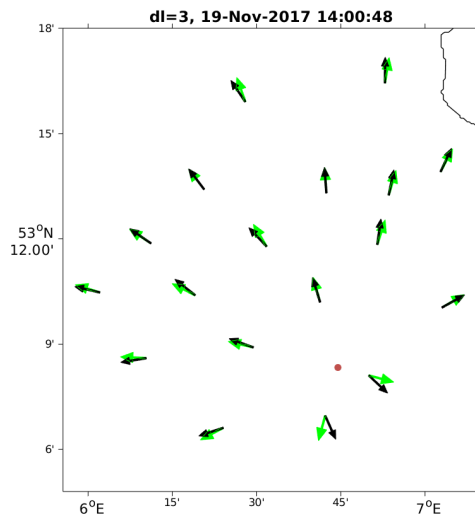


Figure 12: Measured polarization of P-waves (black arrows) and radial polarization of P-waves (green arrows) for a 1D subsurface and an epicentre at the red dot (3D EDT solution). When there is an excellent match between the two, the green arrows are overlain by the black ones.

4 Magnitude

For the computation of the event magnitude, we use the 3D EDT location (Table 1) and the assumption that the hypocentre is just within the chalk. The seismic moment magnitude is computed in 4 steps:

1. The low-frequency spectral level Ω_o is determined at 5 nearby stations.
2. Using Ω_o , the geometry of the problem, impedances at the source and receivers and an assumed attenuation, the released seismic moment M_o is computed.
3. Seismic moment is mapped to moment magnitude M_w .
4. Over the 5 estimates (stations) the average M_w and its standard deviation are computed.

For computing the low-frequency spectral level Ω_o we follow the recipe in *Dost et al.* (2018). Within a frequency band with sufficient signal-to-noise ratio (> 5 dB) the observed amplitude spectrum density is fitted with an adaptation of Boatwrights' source model including an attenuation term (equation 13 in *Dost et al.* (2018)). Fig. 13 shows the amplitude spectra at geophones G524 and G574 and fits of the source-attenuation model parameterized by Ω_o , corner frequency f_c and attenuation parameter t^* .

Subsequently, an adaptation from equation 15 in *Dost et al.* (2018) is used to estimate M_o :

$$M_o = \Omega_o 4\pi r \rho_r^{1/2} \rho_s^{1/2} v_s^{5/2} v_r^{1/2} e^{2\pi f_o t/Q} / 0.64, \quad (1)$$

where ρ_r and v_r are the density and S-wave velocity at the receivers. We use local North Sea Group values of 2040 kg/m³ and 500 m/s, respectively. ρ_s and v_s are the density and velocity at the source. We use values at the upper part of the Chalk Group of 2200 kg/m³ and 1600 m/s, respectively (*Romijn, 2017*). r is the source-receiver distance.

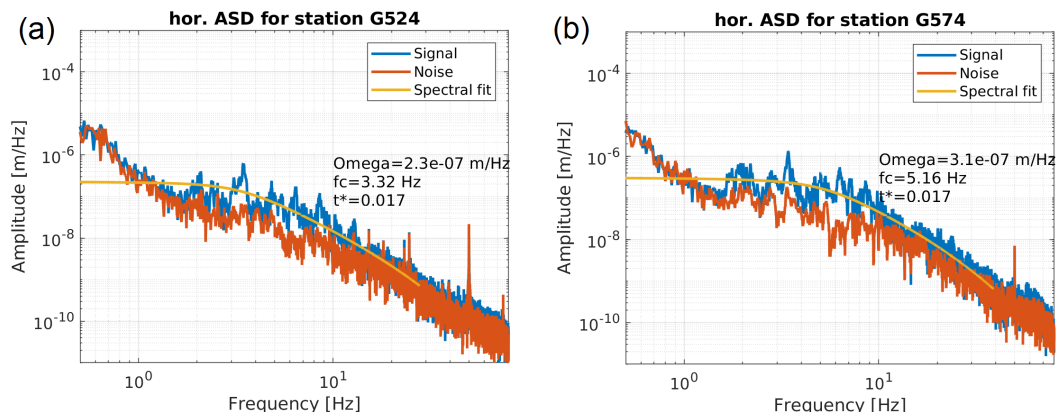


Figure 13: Amplitude spectrum densities (ASD) for geophones (a) G524 and (b) G574 and best-fitting values for the low-frequency spectral level (Ω_o), the corner frequency (f_c) and an attenuation term (t^*) The ASD is averaged over both horizontal components

In comparison with the relation in *Dost et al.* (2018) a factor of 2 has been removed. In our geometry neither the source nor the used geophones are at the free surface and hence no free-surface effect needs to be taken into account. Moreover, an attenuation term has been added to account for anelastic attenuation. We use a Q-factor of 200 at a center frequency $f_0 = 5$ Hz. Lastly, as in *Dost et al.* (2018) we use an average S-wave radiation term of 0.64.

The computed M_o values are mapped to M_w values with

$$M_w = \frac{2}{3} \log_{10}(M_o - 9.1). \quad (2)$$

Over the 5 estimates (stations) this results in $M_w = 1.28 \pm 0.08$.

5 Resonance analysis

If there was a seismic source in, or close to, one of the salt caverns, a resonating wave is expected, which frequency is related to the dimensions of this cavern. In this section we study the frequency spectra of the recordings, to identify resonances and analyze whether there could be a match with one of the salt caverns.

There are 12 salt caverns in the Heiligerlee salt dome, labeled HL-A to HL-M. The figures in Appendix A show the locations and dimensions of the salt caverns. Most caverns look like vertical cigars (Figs. A.2&A.3) with a diameter less than 150 m (Fig. A.1). The caverns have been mined in the salt, between depths of about 700 and 1600 m. All caverns, except for HL-K, are filled with brine and are operated by Akzo Nobel. HL-K is largely filled with nitrogen gas and is operated by GasUnie. The nitrogen column is 487 m, on top of 7 m of brine (*de Buhr et al.*, 2017). At a depth of 1445, the maximum diameter of 68.8 m is reached. Most caverns do not reach depths larger than 1400 m. Two caverns reach deeper: HL-K (1508.0 m) and HL-M (1624 m) Most Heiligerlee salt caverns have vertical extensions larger than 400 m (Figs. A.2&A.3). HL-H and HL-M are exceptions. HL-H is irregularly shaped. Its main shaft has a vertical extension of 215 m. HL-M has seen a large increase in its vertical dimension between the last two measurements (26-04-2007 and 26-03-2014). By 26-03-2014, the cavern had reached a vertical extent of 119 m. Likely the cavern height has increased since.

Fig. 14 shows amplitude spectra for 8 stations nearby the Winschoten event. The spectra have been made for the first 10 seconds of the main event, by averaging over all depth levels and components per station. Notable is a peak at 3.4 Hz, which can be observed at all stations. Also there is a peak at 6.3 Hz that can be seen at most stations.

The Winschoten event is dominated by the 3.4 Hz peak. This cannot be explained as a local propagation feature, since there are large variations in subsurface structure over the used seismic array. E.g., resonance might occur over the receiver-side North-Sea Group (NSG) sediments. However, the depth of the NSG varies widely over the area (Fig.2b), which would result in a varying resonance per site. Also, the 3.4 Hz resonance can be seen on all components. This is another reason to assume that the resonance is not related to wave propagation away from the source. Instead, the 3.4 Hz resonance is likely caused by a structural feature in the source area.

A hypothesis of structure causing the resonance would be a salt cavern. The Heiligerlee caverns are filled with fluid or gas, resulting in a large impedance contrast with the surrounding halite. If a source is at the direct vicinity of such a cavern, reverberating waves could be partly trapped, leading to resonances. The fundamental resonance f_0 would be the same as in a closed pipe:

$$f_0 = \frac{v}{2d}, \quad (3)$$

where v is the velocity inside the pipe and d the (main) dimension of the pipe over which the waves are reverberating.

At pressures and temperatures in Heiligerlee caverns, brine is assumed to have a P-wave velocity of 1830 m/s (*de Buhr et al.*, 2017). If a brine filled cavern were to act as a resonating pipe, the resonating length scale d_{brine} (for a $f_0 = 3.4$ Hz) would be (using Equation 3) $d_{brine} = v_{brine}/(2f_0) = 269$ m.

In cavern HL-K, nitrogen was measured to have a P-wave velocity of 404.3 to 409.2 m/s (*de Buhr et al.*, 2017). Assuming this nitrogen-filled cavern as a resonating pipe, and using a velocity of 407 m/s, the dimension that would result in a $f_0 = 3.4$ Hz resonance would be $d_{nitrogen} = 60$ m.

None of the brine filled caverns can explain a 3.4 Hz resonance by reverberations in the horizontal direction, as a width of about 269 m would be needed, and the maximum diameter is about 150 m (Fig. A.1). The nitrogen filled cavern HL-K, has a maximum diameter of 68.8 m. That is close to the dimension that could explain a 3.4 Hz resonance for a gas-filled cavern (60 m).

Most brine-filled caverns are too high to explain a 3.4 Hz resonance by reverberations in the vertical direction. Cavern HL-H has a main height dimension of 215 m, which is considerably smaller than the value computed (269 m). Cavern HL-M was too small at the date of its last measurement (119 m at 26-03-2014). Potentially it was large enough by 19-11-2017 to yield a 3.4 Hz resonance.

Waves resonating within a cavern would be P-waves. The 3.4 Hz resonance is also strongly seen on the radial component and also somewhat on the transverse component (Figs. 5–7). This observation is not expected for a primarily P-wave resonator, unless strong P-S conversion takes place at the edges of the resonator.

Alternatively, a resonance might occur at the base of the NSG. About halfway the NSG a stiffer formation is present: the Brussels Sand. In the source area, waves could be bouncing back and forth between the top Chalk and base Brussels Sand. Assuming the lower NSG

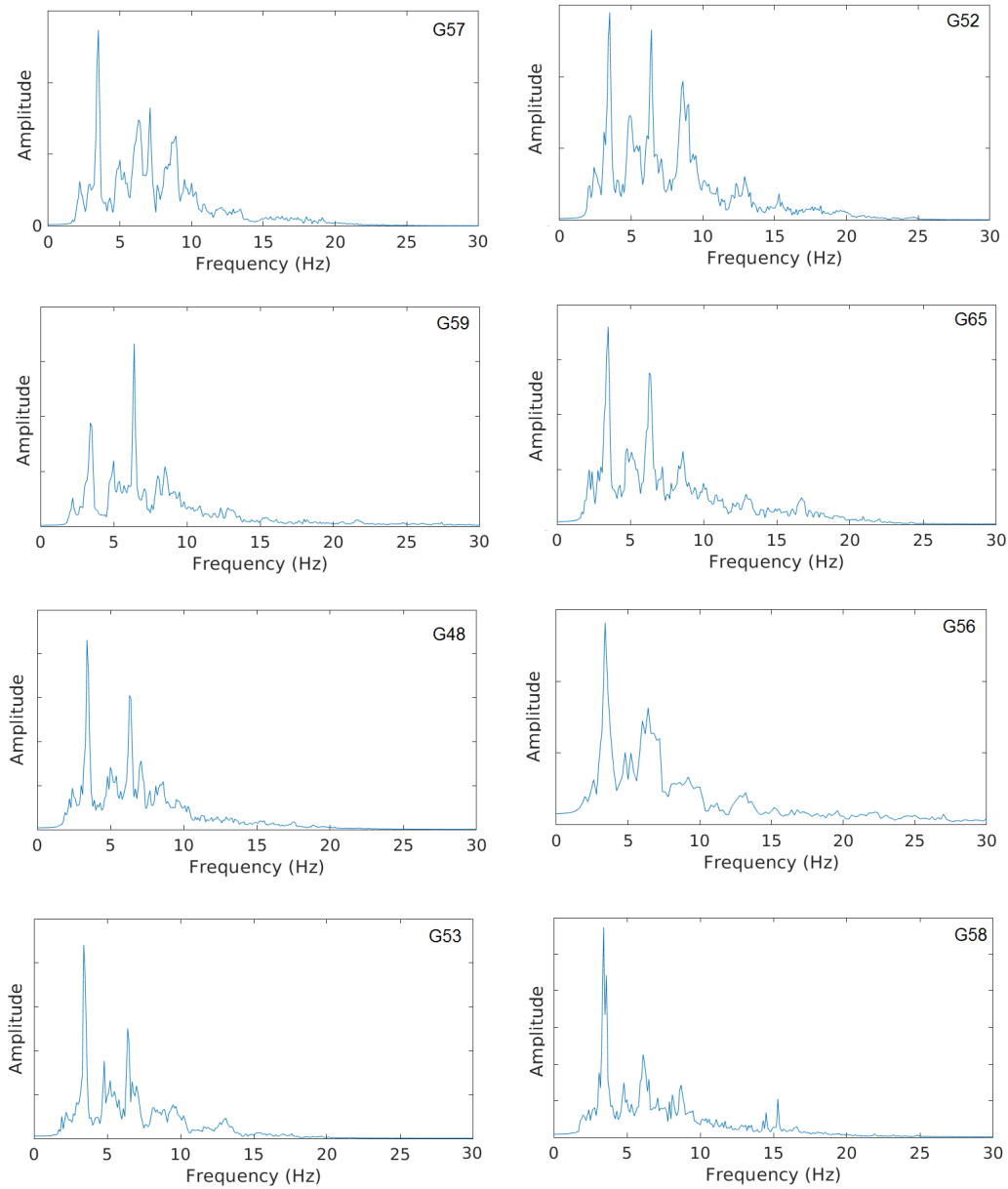


Figure 14: Stack of amplitude spectra per station, for the first 10 second time window of the main Winschoten event. For each station (name is given in the upper right of graphs) the amplitude spectra of all depth levels and components were stacked.

to be the resonator, and using a P-wave velocity of 2000 m/s (Romijn, 2017) the dimension that would result in a $f_0=3.4$ Hz resonance would be 290 m. This value would be in the range of expected thicknesses of the lower NSG. The exact depth of the base of Brussels Sand, however, is not known at this location.

6 Scanning for similar events

The Winschoten 19-11-2017 events were the only events near Heiligerlee that were automatically detected with the dense G-network (*Dost et al.*, 2017) that is operational from 2015. There could have been smaller events that were missed, prior or after the detected event on November 19. In this section we apply an automatic scanning algorithm to search for similar events.

The KNMI receives near real-time data streams of more than 500 seismic sensors. On this data stream, an automatic picker is running that detects transients. When 6 or more detections are made within a limited time window, an automatic location algorithm is started. Using a threshold of 6 circumvents a large amount of 'false' detections caused primarily by anthropogenic seismic noise, which sometimes happens to be concurrent on multiple sensors. This threshold of 6, however, precludes the observation of smaller seismic events that were only detected at a few stations. Such events are only later detected by the analyst when he/she goes through lists of possible events with <6 detections, or with an automatic scanning algorithm. We select the sensor with the best signal-to-noise ratio for the main event, that is G574, the 200 m depth level geophone of station G57. For this sensor we scan through the data from November 5 until December 3 (2 weeks prior to 2 weeks after the main event). We start off with visually inspecting high resolution spectrograms and continue with implementing a scanning algorithm.

6.1 Spectrograms

Fig. 15 shows two spectrograms for November 19: one for geophone G574 on top of the Heiligerlee dome, and one 'reference' spectrogram at geophone N024, which is located 38 kilometer to the WSW. On these spectrograms continuous noise sources can be identified as horizontal features, e.g., the strong upper tail of the microseism between 0.1 and 1 Hz. This noise source is relatively weak on G574 thanks to its somewhat shielded dome setting. Besides noise, also transient events can be identified on the spectrograms, as vertical yellow lines: short duration recording of seismic energy within a large frequency bandwidth. On both spectrograms, 3 teleseismic arrivals are visible between 0.1 and 1 Hz. Only for station G574, the Winschoten event is visible, between about 3 and 80 Hz. With a red arrow another event is highlighted. This is an event of unknown origin. It could be related to the Winschoten events. It could also have a completely different origin. It is not visible on N024, neither on the next closest station to G574, which is G524. This makes it difficult to find an origin for this minute event.

Scanning through the 29 days with spectrograms alike Fig. 15, a few more suspect events were found at G574, without recordings at other nearby stations. In the following we apply a scanning algorithm that also identifies smaller events and inherently incorporates association with the main event, if present.

6.2 Template matching

In Section 2 it was observed that the Winschoten event is in fact a succession of at least 4 subevents. These subevents are labeled in Fig. 16 with W1, W2, W3 and W4. A time window around each such subevent could serve as a template. These templates are used to

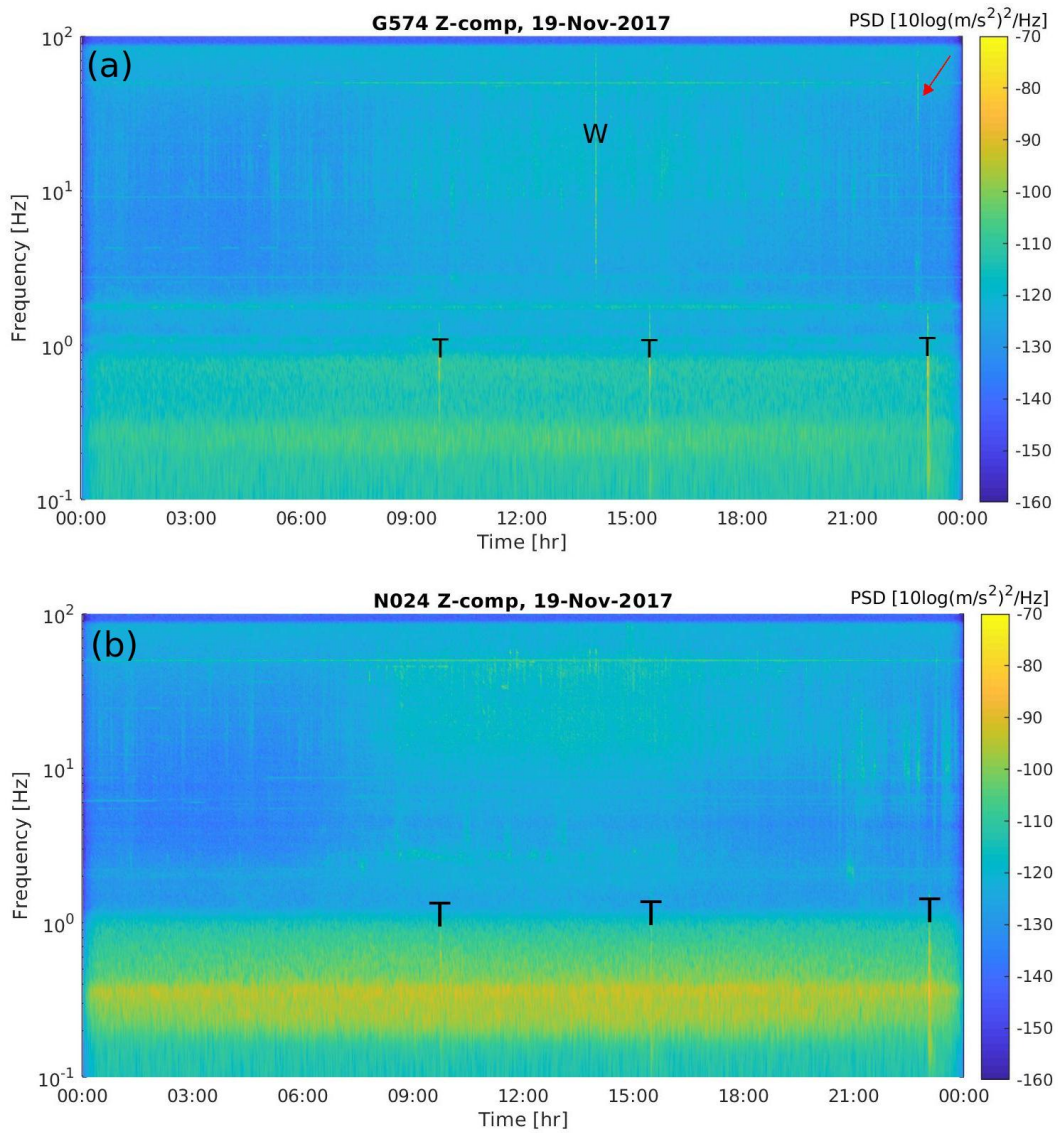


Figure 15: Spectrograms for vertical-component recording of geophone (a) G574 and (b) N024. Geophone G574 is located on top of the Heiligerlee dome, whereas N024 is located near the village of Norg, 38 km WSW of station G574. The Winschoten event is denoted with 'W', 3 teleseismic events are denoted with 'T'. The red arrow highlights a very local event with unknown origin.

6.2 Template matching

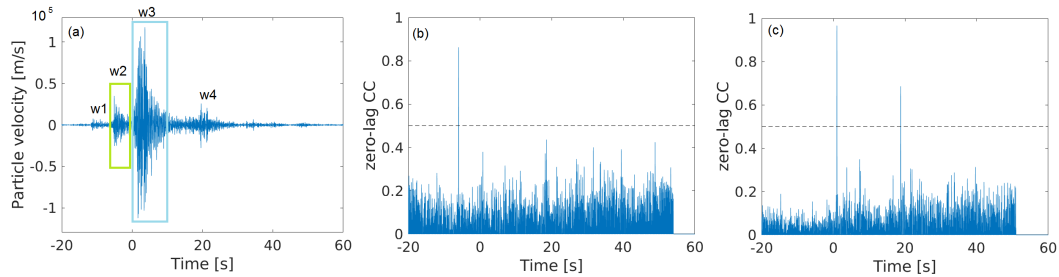


Figure 16: (a) Winschoten event with the 4 subevents labeled: W1,W2,W3 and W4. (b) and (c) show matching results of W2 and W3, respectively, with the 80 seconds recording as shown in (a). A matching is obtained when a cross-correlation coefficient is obtained larger than 0.5.

scan through the continuous data to find similar recordings, which would hint at a source with similar origin.

The template matching is implemented as a zero-lag cross-correlation (CC). From the 3 components, the East component recorded the Winschoten events with the largest SNR. Hence, this component is used for the template matching. A template event is obtained by time windowing and energy normalization. Subsequently, from the continuous data stream a time window is taken with the same duration. Also this time window is energy normalized. Next, the two time windows are cross-correlated and the zero-lag CC is stored. Then, the time window is shifted by one sample, and the process is repeated, yielding a continuous stream of CC values. The zero-lag CC in combination with energy normalization yields high matching values, irrespective of the amplitude difference between master and slave waveforms.

Events that differ in magnitude have different corner frequencies. This negatively affects the similarity of the waveforms. To mitigate this effect, a soft whitening is applied prior to cross-correlation and energy normalization.

W1 is recorded just above the noise floor. It turns out to have insufficient signal-to-noise ratio (SNR) to serve as a template. A window around W2 is selected (Fig. 16(a), light green) and used as template. Fig. 16(b) shows the result of the template matching for the same time window of data as shown in Fig. 16(a). Only the timing of W2 pops up as a large peak in the CC values. At all other times, the scanner yields levels significantly lower than the threshold of 0.5. Fig. 16(c) shows the result of scanning with W3 (Fig. 16(a), cyan), as a template. A match (CC value larger than 0.5) is obtained at the actual timing of W3, but also at the timing of W4. Hence, it turns out that events W3 and W4 have a large similarity.

The scanning is upscaled to the entire day, resulting in the plots as shown in Fig. 17. In this figure, only high peaks can be seen at times corresponding to the known Winschoten events; this day no other occurrences exist of events from the same source region and with similar focal mechanism. Hence, the event highlighted with the red arrow in Fig. 15(a) is not a repetition of one of the Winschoten (sub)events.

The scanning is further up scaled to two weeks prior until two weeks after November 19, 2017. A few more events are found with similarities just above the threshold of 0.5. These are listed in Table 2&3, for templates W2 and W3, respectively.

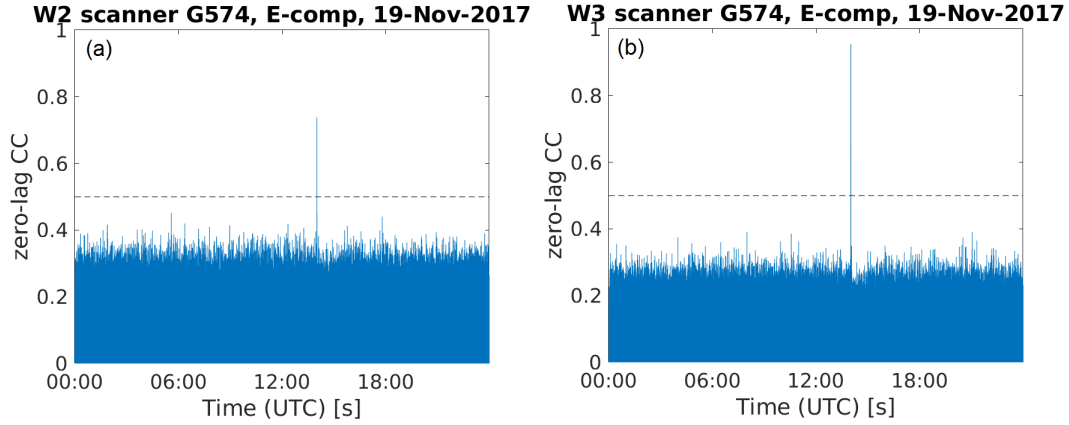


Figure 17: Results of scanning through 1 day of continuous data with templates (a) W2 and (b) W3 (templates have been defined in Fig. 16(a)). A zero-lag cross-correlation (CC) coefficient of more than 0.5 means that a similar event was recorded.

Number	Time [UTC]	CC coefficient	Max. amplitude [μ/s]
1	11 Nov 2017 08:27:40	0.51	0.118
2	13 Nov 2017 08:26:41	0.51	0.425
3	16 Nov 2017 04:34:39	0.54	0.0659
4	19 Nov 2017 14:00:42	0.79	2.91
4	30 Nov 2017 14:16:08	0.51	2.254

Table 2: Occurrences between Nov. 5 and Dec.3, 2017, of arrivals with high similarity (CC coefficient >0.5) with respect to W2 (Fig. 16a). The template event is made bold.

Number	Time [UTC]	CC coefficient	Max. amplitude [μ/s]
1	17 Nov 2017 16:00:57	0.52	0.786
2	19 Nov 2017 14:00:49	0.94	10.9
3	19 Nov 2017 14:01:06	0.65	2.33

Table 3: Occurrences between Nov. 5 and Dec.3, 2017, of arrivals with high similarity (CC coefficient >0.5) with respect to W3 (Fig. 16a). The template event is made bold.

7 Monitoring

For detailed seismic monitoring of the Heiligerlee salt dome, currently there is no dedicated network, to allow both detection and location of minute seismic events. The implemented scanning approach (Section 6) would not be sufficient as a monitoring tool. Events are likely to occur for which a template does not (yet) exist. As an alternative (temporary) monitoring tool, in this section we evaluate the use of simple amplitude tracking.

In the two salt cavern collapses described in the literature (*Shemeta et al., 2013; Kinscher et al., 2014*) a large amount of seismicity was observed prior to the actual collapse. If such collapse would be imminent in the Heiligerlee or Zoutwending dome, also a similar build-up of seismicity is to be expected. This seismicity likely stands out from the cultural noise, especially at KNMI geophones at 200 m depth, where highfrequency surface waves ($\lesssim 2$ Hz) do not penetrate. Hence, keeping track of seismic amplitude levels at these depth could serve as a first-order monitoring tool.

We consider to keep track of root-mean-square (RMS) amplitudes at the most nearby geophones. For Heiligerlee, there is a geophone both at the northern edge (G524: [lat, lon]=[53.1699, 6.9837]) and southern edge (G574: [lat, lon]=[53.1351, 7.0222]) of the dome. For Zuidwending, there is a geophone at the northern side (G584: [53.1103, 6.9071]) of the dome. At the other side of the dome, a LOFAR site exists: Alteveer, with 7 geophones at depth levels between 30 and 120 m. The instrument cabinet at this site has been molested. Bringing the site back online would involve an investment to restore the cabinet.

Fig. 18 shows RMS amplitudes computed for geophone G574 for one week in November. The last day of that week, on 19-11-2017, the events near Winschoten occurred. These events clearly stand out in respect of RMS amplitude. The events happened midday on a Sunday, when there was little cultural noise. On all week days there is strong cultural noise, especially during day time. During the night, and also in the weekend, the seismic noise conditions are more favorable. At the analyzed site, only the latter times could be used to detect possibly anomalous seismic activity.

One USArray station (544A) monitored the seismic activity prior to the Grand Bayou cavern collapse in Louisiana, USA (*Shemeta et al., 2013*). This data is publicly available and could be used to test a simple RMS-based tool as an indicator of possibly hazardous situations.

8 Conclusions

A succession of at least 4 events was measured on November 19, 2017, northeast of the city of Winschoten. The largest amplitude was recorded at sensor G570: a peak particle acceleration of 2.45 mm/s. The P- and S-waves of the main event could be picked at 6 and 2 stations, respectively. With a jack-knife test one P-wave pick was removed. First a time-difference localization with the 5 remaining P-wave picks was implemented to constrain the epicentre. Subsequently, P-S delay times were used to constrain the depth. The source was found to be located at a depth of maximum 1.5 km. Hence, a location within the underlying gas reservoir could be ruled out. Later, the localization was improved by using a detailed 3D velocity model, a 3D ray tracer, and a P-wave time-difference scheme. The main event was mapped to a location in the (lower) North Sea Group or upper Chalk Group, above the western flank of the Heiligerlee salt dome. At this location, brittle rock overlying the salt could have moved due to salt creep. The uncertainty ellipse includes the part of the salt dome where the caverns are present. However, a hypocentre at the depth range of the caverns is unlikely.

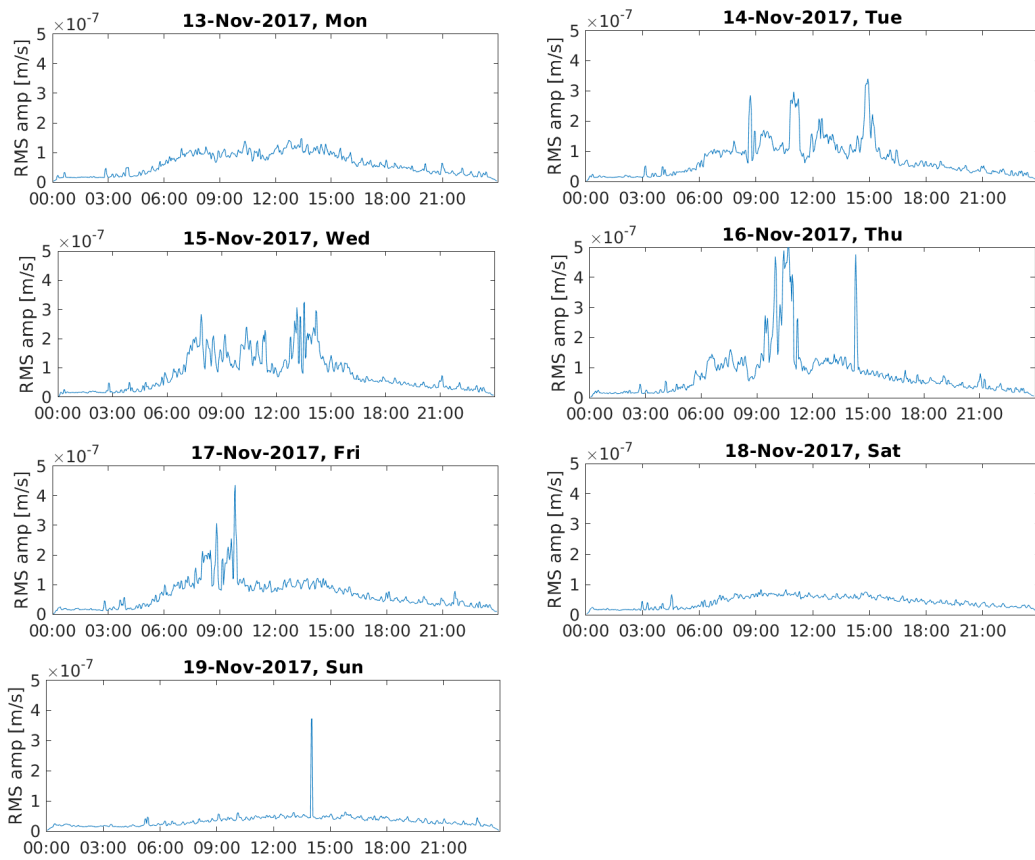


Figure 18: Root-mean-square (RMS) amplitudes of the vertical component at station G57 for one week of continuous data bandpass filtered between 5 and 40 Hz. The RMS amplitude is computed over a sliding widow of 300 seconds, with a 50% overlap.

We computed a moment magnitude for the largest event, using the horizontal component amplitude spectra at the 5 most nearby stations. With the assumption that the source is just within the Chalk Group, a moment magnitude of 1.28 ± 0.08 was found.

All nearby KNMI seismic stations recorded a strong 3.4 Hz resonance for the event. This resonance likely originated in the source area. At the Heiligerlee salt dome, 12 caverns have been mined. The assumption was tested whether one of the salt caverns would act as a resonating closed pipe. From the 12 caverns, 2 can possibly generate the recorded resonance: brine filled caverns HL-M over its height and nitrogen-filled cavern HL-K over its width. This list of 2 could be further restricted by finding the current height of cavern HL-M. After the improved location using the 3D velocity model, a source location within the salt dome is unlikely. Another hypothesis to explain the resonance would be waves trapped between the Brussels Sand and Chalk in the source area.

Waveforms two weeks prior to two weeks after November 19 were scanned to find possible similar, but smaller, events, that would have been missed in the standard processing at KNMI. The two largest subevents (W2 and W3) were used as a template. The scanning resulted in a few records with similarities just above the threshold of a 0.5 correlation coefficient. Subevent W4 turned out to be a close match to W3, with a correlation coefficient of 0.65. No signs are seen of a build-up of seismicity.

The implemented scanning approach would not be sufficient as a monitoring tool. Events are likely to occur for which a template does not (yet) exist. For detailed seismic monitoring of the Heiligerlee salt dome, currently there is no dedicated network, to allow both detection and location of minute seismic events. As a (temporary) alternative, we would suggest a monitoring tool solely based on sliding windows of root-mean-square amplitudes. With such a tool, minute events during the day will be missed due to high cultural noise levels, but a build-up of seismicity, if present, would be captured.

References

- de Buhr, A., L. Wendt, P. Ernst, and A. von der Heyde (2017), Echo-log Heiligerlee K, *Sonar Control Kavernenvermessung GmbH (SOCON)*, 8. Survey, 20-12-2017, 174 097.
- Dost, B., E. Ruigrok, and J. Spetzler (2017), Development of probabilistic seismic hazard assessment for the Groningen gas field, *Netherlands Journal of Geosciences*, 96(5), s235–s245, doi:10.1017/njg.2017.20.
- Dost, B., B. Edwards, and J. J. Bommer (2018), The relationship between m and m_l : A review and application to induced seismicity in the Groningen gas field, the Netherlands, *Seismological Research Letters*, 89(3), 1062–1074.
- Hofman, L., E. Ruigrok, B. Dost, and H. Paulssen (2017), A shallow velocity model for the Groningen area in the Netherlands, *Journal of Geophysical Research: Solid Earth*, 122, 8035–8050, doi:10.1002/2017JB014419.
- Kinscher, J., P. Bernard, I. Contrucci, A. Mangeney, J.-P. Piguet, and P. Bigarre (2014), Location of microseismic swarms induced by salt solution mining, *Geophysical Journal International*, 200(1), 337–362.
- KNMI (1993), Netherlands Seismic and Acoustic Network, Royal Netherlands Meteorological Institute (KNMI), Other/Seismic Network, doi:10.21944/e970fd34-23b9-3411-b366-e4f72877d2c5.

- Lienert, B. R., E. Berg, and L. N. Frazer (1986), HYPOCENTER: An earthquake location method using centered, scaled, and adaptively damped least squares, *Bulletin of the Seismological Society of America*, *76*(3), 771–783.
- Lomax, A. (2005), A reanalysis of the hypocentral location and related observations for the great 1906 california earthquake, *Bulletin of the Seismological Society of America*, *95*(3), 861–877.
- Romijn, R. (2017), Groningen velocity model 2017, *Tech. rep.*, NAM (Nederlands Aardolie Maatschappij).
- Shemeta, J., M. Leidig, and D. Baturan (2013), Passive Seismic Observations at Grand Bayou, Louisiana, USA Associated with the Failure of the Oxy Geismar #3 Solution Cavern, SMRI Fall Conference 2013, Avignon France 30 September-1 October, pp. 143-152.
- Snieder, R., and M. Sambridge (1992), Ray perturbation theory for traveltimes and ray paths in 3-D heterogeneous media, *Geophysical Journal International*, *109*(2), 294–322.
- Spetzler, J., E. Ruigrok, and B. Dost (2018), Improved 3D hypocenter method for induced earthquakes in Groningen, Nederlands Aardwetenschappelijk Congres, March 15-16. Veldhoven, the Netherlands.
- Stockwell, R. G., L. Mansinha, and R. Lowe (1996), Localization of the complex spectrum: the S transform, *IEEE transactions on signal processing*, *44*(4), 998–1001.
- Tarantola, A. (2005), *Inverse Problem Theory and Methods for Model Parameter Estimation*, SIAM, Philadelphia.
- Van Dalzen, W., J. Doornenbal, S. Dortland, and J. Gunnink (2006), A comprehensive seismic velocity model for the netherlands based on lithostratigraphic layers, *Netherlands Journal of Geosciences*, *85*(4), 277.

A Heiligerlee salt caverns layout



Royal Netherlands Meteorological Institute

PO Box 201 | NL-3730 AE De Bilt
Netherlands | www.knmi.nl